Effects of shot-peening and stress ratio on the fatigue crack propagation of AL 7475-T7351 specimens

N. Ferreira[a], P.V. Antunes[a*], J.A.M. Ferreira[a], J.D. Costa[a], C. Capela[a,b]

[a] CEMMPRE, University of Coimbra, Department of Mechanical Engineering, Rua Luís Reis Santos, 3030-788, Coimbra, Portugal.
[b] Instituto Politécnico de Leiria, ESTG, Department of Mechanical Engineering, Morro do Lena – Alto Vieiro, 2400-901 Leiria, Portugal

Abstract

Shot peening is an attractive technique for fatigue enhanced performance of metallic components, because it promotes crack initiation retardation and later crack growth. Engineering design based on fatigue crack propagation predictions applying the principles of fracture mechanics is commonly used in aluminum structures for aerospace engineering. The main purpose of present work was to analyze the effect of shot peening on the fatigue crack propagation of the 7475 aluminum alloy, under both constant amplitude loading and periodical overload blocks. The tests were performed on 4 and 8 mm thickness specimen`s with stress ratios of 0.05 and 0.4.

The analysis of the shot-peened surface showed a small increase of the micro-hardness values, due to the plastic deformations imposed by shot peening. The beneficial effect of surface peening on fatigue crack growth rates is quite limited to an increasing near the threshold. The specimens' thickness has only marginal influence on the crack propagation, in opposite to the stress ratio. Periodic overload blocks of 300 cycles promotes a reduction of the fatigue crack growth rate for both intervals of 7,500 and 15,000 cycles.

Keywords Aeronautical aluminum alloys, Fatigue crack propagation, Overloads, Shot peening, Paris law.

Peer-reviewed version available at Appl. Sci. 2018, 8, 375; doi:10.3390/app8030375

1. Introduction

High-strength aluminium alloys are widely used in aerospace applications due to the high strength-to-weight ratio, good corrosion resistance and high toughness combined with good formability and weldability. One of the principal problems in contemporary aircraft industry is to ensure simultaneously reliability, high durability, minimum weights and economic efficiency of transport airplanes. In order to get such aircraft characteristics, it is required to design the structure ensuring high damage tolerance. The approach to engineering design based on the assumption that flaws can exist in any structure and cracks propagate in service, is commonly used in aerospace engineering. Therefore, the prediction of crack growth rates based on the application of fracture mechanics theory is an important aspect of a structural damage tolerant assessment.

Many metal components, like turbines blades, used in aerospace and power industries are subjected to dynamic mechanical loading, leading to the initiation of fatigue cracks. One way to reduce the risk of fatigue crack initiation is to introduce compressive stresses in the region of higher stresses concentration, for example by shot peening. This is a well-established surface treatment technology at the industrial level, despite generating a significantly rougher surface with associated surface defects [1]. Since the majority of fatigue cracks initiate on the surface, the conditioning of the surface to resist crack initiation and earlier crack growth is a practical method of improving fatigue performance. The indentation of each impact, in shot peening process, produces local plastic deformation given rise to a field of surface compressive stresses. Studies by many researchers have shown a positive shot peening effect [2-4], resulting from the introduction of residual compressive stresses in the subsurface layers of material. Depending on the peened material there is an Almen intensity for which the optimum fatigue strength is achieved, corresponding to a certain balance between residual compressive stress field and surface roughness damage.

Paris`s law, which relates fatigue crack growth rate (da/dN) and the stress intensity range (ΔK) is the prime approach adopted for characterizing fatigue crack propagation in engineering structures. The fatigue crack growth of the aluminum alloys in the Paris`s law regime is affected by microstructure [5-7] and by the crack closure induced by

plasticity, oxidation and surface roughness (in the near threshold regime). The influence of mean stress on the fatigue crack growth rate has been explained with success by crack closure [6, 8]. Bergner and Zouhar [6] showed that crack growth rates of various aluminium alloys varied by a factor of about 20 for some ΔK values, suggesting that the main factor to explain that discrepancies was the crack closure effect and the environment. Fatigue cracks inevitably grow into a material region which has suffered large plastic strains due to its location in the crack tip plastic zone. As a rule, this material is plastically stretched in the direction normal to the crack flanks. This plastic deformation is left in the wake of the crack. It acts similarly to an additional wedge grouted between the flanks, thus pre-straining them and partly shielding the crack tip from the action of subsequent loads. This phenomenon is called plasticity induced crack closure and tends to decrease the effective stress intensity range thereby resulting in slower crack propagation rates [8].

In compact tension (CT) specimens the crack progresses more rapidly in center than at the surface conducting to a crack tunneling effect, due to the prevailing tri-axial state of stress at the center, promoting plain strain in contrast with plain stress at surface. Striation spacing between beach marks on fatigue crack surfaces is also affected by shot and laser peening effect. Zhou *et al.* [9] have observed a decrease in striation spacing with increase in the number of laser peening impacts for Ti6Al4V specimens'. For the same alloy, B.K. Pant *et al.* [10] studied the effect of shot peening and laser peening on the fatigue crack propagation and compared with the untreated one with respect to the striation spacing for R = 0.1 and R = 0.7, both peening surfaces presented a reduction on the striation spacing when compared to the untreated specimens.

Overloads can lead to significant interaction effects on crack propagation, as have been reported in many [11-22]. Several mechanisms have been proposed to explain crack growth retardation; including models based on residual stresses, crack closure, crack tip blunting, strain hardening, crack branching and reversed yielding. The effect of residual plastic deformation leads to compressive stresses in the wake of the crack and raises the crack opening load on subsequent crack growth (crack closure), becoming the most important phenomena in explaining the variation of the characteristic features of post-overload transients [19–23]. Donald and Paris [23] observed for 6061-T6 and 2024-T3

aluminium alloys, that closure measurements produced a good data correlation between different stress ratio crack growths obtained with K-increasing conditions. However, in the near-threshold regime with crack growth data obtained by the K-decreasing procedure, the measured opening loads were excessively high. This discrepancy was justified by Paris *et al.* [24] which proposed the ‘‘partial closure model’’. Borrego *et al.* [25] concluded that crack closure was able to explain the influence of the stress ratio on the fatigue crack growth rate for the 6082-T6 aluminium alloy and the influence of several load parameters for overloads interactions if the partial crack closure model is included in the analyses.

The present work analyzes the effect of: shot peening, specimen thickness and stress ratio on the fatigue crack propagation of 7475 aluminum alloy with T7351 heat treatment. A more extensively analysis of the crack growth following periodical tensile overloads blocks is also evaluated.

2. Materials and experimental procedures

2.1. *Materials and samples*

This research was conducted using the 7475 aluminum alloy with a T7351 heat treatment. 7475 aluminum alloys are widely used in aeronautical applications where the combination of high strength, fracture toughness, good fatigue crack propagation and corrosion resistance are required. The chemical composition is shown in Table 1. According to the material manufacturer, the ultimate tensile stress and yield stress are σ_{UTS} = 490 MPa and σ_{YS}= 414 MPa, respectively.

In order to study the effect of the surface shot peening on crack propagation two CT specimen’s batches were prepared: one with shot peening (SP) and another without shot peening but with the lateral surfaces mechanically polished (MP).

MP specimens were polished to ensure a good visualization of crack propagation. Manual grinding was done with a LaboPol-5 – Struers A/S, DK-2750, machine passing progressively the grinding papers 240, 320, 600, 1000 and 2500. After the specimens grinding diamond paste of 3μm and 1μm were used in order to give the specimens a mirrored surface aspect.

Shot peening was done in OGMA -Indústria Aeronáutica de Portugal S.A. company with a large experience in producing components and aeronautics repair. Both sides of the specimen were subjected to a manual shot peening process, using a SURFATEC machine, shown in Fig. 1a), and an Almen strip type A, according to SAE J443 standard [26]. Coverage was assessed by visually inspecting the surface, using a 10x magnifying lens. The coverage is achieved at 100% when this analysis shows a surface completely attained by the particles. The beads used in current study were of the type S170 with 0.43 mm diameter and Almen type A with intensity 0.20A [mm], according SAE AMS2430 standard [27] for aluminum alloys. Fig. 1b) shows one sample after the shot-peening process.

The studies of fatigue crack propagation were performed using the standard Compact Tension (CT) specimen with the geometry shown in Fig. 1c), according with ASTM E647 standard [28]. For each batch of specimens two different thickness (B) were manufactured: 4 mm and 8 mm. The specimens were machined in the longitudinal transverse (LT) direction from laminated plates. For each test condition three specimens were used.

The surface roughness was evaluated according to DIN EN ISO 4288 standard [29] using a Surftest SJ-500 Mitutoyo, surface roughness measuring system. The parameters evaluated for each superficial treatment were: roughness average R_a, root mean square (RMS) roughness R_q and mean roughness depth R_z. Table 2 summarizes the roughness parameters showing an increasing of more than 300% in the three roughness parameters for the peened surfaces.

In order to analyze the material microstructure, some samples were cut through the cross section. Afterwards, the surfaces were gradually polished with smaller granulometry silicon carbide papers, and at the end diamond particles with a 1 μm diameter were used until it became a mirror-like surface. Then, the surfaces were etched with Keller reagent (2.5% HNO_3; 1.5% HCl; 1% HF; 95% H_2O [volume]) and taken micrographs using an optical microscope Leica DM 4000 M LED. Fig. 2 shows typical micrographs indicating that base material microstructure (fig 2a) consists of grains

elongated in the rolling direction. Around shot peened surface (fig. 2b) an increasing of grain deformation and roughness was observed.

Surface Vickers hardness tests were performed according to ASTM C1327 -15 [30] using a Struers Duramin micro-hardness tester with 0,5 N load for 15 seconds. Micro-hardness measurements were done at 0.3 mm from the surface, and spaced out 0,5 mm, for both specimens type, MP and SP. The average values obtained from twenty measurements, were: $HV_{0.05}$ = 157 for MP surfaces and $HV_{0.05}$ = 167 for SP surfaces. Therefore, shot peening surface hardness increased is more than 6%.

Residual stresses were measured, in-depth and on the longitudinal surface. The analysis was performed by X-ray diffraction using a Proto iXRD equipment. Lattice deformations of the {222} diffraction planes were measured using Cr-Kα X-ray radiation, with 22º ψ angles, in the range ±42°, an acquisition time of 30 seconds by peak and ±2° oscillations in ψ. For the analyzed material and considering the radiation used, the average penetration depth of the X-rays was about 11 µm.

2.2. Fatigue tests

Fatigue crack propagation tests were carried out, in agreement with ASTM E647 standard [28], using 4 and 8 mm thick compact specimens (CT). The tests were performed under load control at room temperature using a 100 kN capacity servo-hydraulic Instron 1341, with a frequency within the range 15–20 Hz and stress ratios of R = 0.05 and 0.4. The specimen's geometry and dimensions are shown in Fig. 1c). For both specimens´ batches two types of tests were carried out: constant amplitude loading tests with the stress ratios R = 0.05 and 0.4 and variable amplitude loading tests in which periodic overload blocks of 300 cycles are applied with intervals of N_{int} cycles as is shown schematically in Fig. 3. The main purpose of these tests is to obtain the *a-N* and *da/dN* curves as a function of the stress intensity factor range ΔK in order to analyze the effects of the shot peening, specimen thickness and stress ratio.

For the surface polished specimens the surface crack length was measured using a travelling microscope (45x) with an accuracy of 10 µm. Crack growth rates under

Peer-reviewed version available at Appl. Sci. 2018, 8, 375; doi:10.3390/app8030375

constant amplitude loading were determined by the incremental polynomial method using five consecutive points [28]. For the surface peened specimens, the crack length was obtained by using experimental calibration curves based on the compliance variation, previously obtained with the polished specimen's tests. Taking in account the compliance (C) definition Equation (1).

$$C=\frac{(u_{máx}-u_{mín})}{(P_{máx}-P_{mín})} \quad (1)$$

where *u* and *P* are the axial grip displacement and the load, respectively, which were monitored during the test. From the non-peened specimen tests with constant amplitude loading it was monitored a set of data for *C* calculation and the correspondent values of the crack length. The collected data are plotted in Fig. 4, in terms of the crack length (mm) *versus* the compliance, and fitted by equations 2a) and 2b) for specimens with 8 mm and 4 mm thickness, respectively, both with a 0.99 correlation factor. These equations were afterwards used for the evaluation of the crack length in the tests with peened specimens and in the periodical overloading block tests.

$$a=39515\times C^5-53199\times C^4+27962\times C^3-7278.2\times C^2+980.36\times C-23.559 \quad (2a)$$

$$a=2905.2\times C^5-6399\times C^4+5393.9\times C^2+2275.3\times C^2+502.82\times C-16.62 \quad (2b)$$

3. Results and discussion

Figs. 5, 6 and 9 highlight the effects of the specimen`s thickness, surface peening and stress ratio *R*, on the crack propagation curves, respectively. Figs. 5 a) to 5 d) show the influence of the thickness on the *da/dN*-Δ*K* curves. It is well known [31], that the thickness influence on the fatigue crack propagation is related both to the microstructure and stress state. In the present study, specimens were machined from the same thickness bars, so there is no microstructure change between 4 and 8 mm thickness specimens. Therefore, the effect of thickness is only caused by changes in stress distribution along cross section and consequent variation on crack closure level [31]. The analysis of Fig. 5 shows a reduced thickness effect on *da/dN* for both surface treatments (MP and SP

specimens), including in the near-threshold region. The higher thickness specimens have higher *da/dN* for the same ΔK values in all conditions analyzed in Fig. 5. It is also possible to notice that for R = 0.05 the increase in *da/dN* is higher with increasing ΔK. Specimen's thickness effect is more noticeable for lower *R*-values and *MP* samples. As expected, independently of the surface treatment the ticker specimens have higher crack growth rates over all the ΔK range analyzed.

The main purpose of current work was the analysis of the surface peening effect on the crack propagation. Figs. 6 a) to 6 d) show the influence of the shot peening on the *da/dN*-ΔK curves for both thicknesses and stress ratios. Taking into account that shot peening has a much localized effect near the surface, which results in the introduction of compressive residual stresses, the propagation of cracks will be affected only in these areas. In order to analyse the retardation of crack propagation around the surface, the fractured specimens were observed by optical microscopy.

Figs. 7a) and 7b) are exemplary photos showing the marks of crack growth shape for machined and shot peening specimens, with 8 mm thickness, respectively. These marks were produced during variable amplitude loading with periodic overload blocks tests. Although the specimen`s thickness is small to ensure tri-axial plain strain conditions in the center of the sample, the crack path presents a significant tunnel effect, as shows Figs. 7a) and 7b), and according also to Zhou *et al.* [9]. The visual observation of the images doesn't show a clear evidence of the shot peening effect on the crack path. For a detailed analysis it was defined a tunnel effect parameter by the relation:

$$tunnell\ effect = \frac{a_2 - \left(\frac{a_1 + a_3}{2}\right)}{a_0}$$

where, a_1 and a_3 are the crack lengths at the specimen´s surfaces, a_2 is the current crack length at the center and a_0 the initial crack length. This parameter is plotted in Fig. 7 c) against the fatigue crack length (a_2 - a_0). As expected shot peening increases the retardation of the surface crack propagation observed by a higher tunnel effect parameter for crack length lesser than 10 mm. As said before, tunnel effect can be caused by residual stresses profiles. For MP specimens average residual stresses in load direction obtained from 4 measurements at the surface was about +290 MPa, while for SP samples

compressive residual stresses occur around the surface. Fig. 8, shows the profile of residual stresses and X-ray diffraction peak breadth against the depth from surface. According, to the diffraction peak breadth profiles, the thickness of the layer affected by all surface treatments is about 200 µm. Compressive residual stresses have an average value of about 200 MPa, in a 150 µm layer bellow the free surface. The reduced thickness of this layer, justifies the reduced influence on the overall propagation of fatigue cracks observed, in accordance to He *et al.* [32].

The results obtained for the two stress ratios R = 0.05 and R = 0.4 are compared in Fig. 9, for both surface treatments and thicknesses. As expected, significant influence of the stress ratio was observed in both Paris law regime and near-threshold condition. As reported in literature this effect is mainly consequence of the significant reduction on crack closure level for the higher stress ratio R = 0.4 [31]. This is why above 15 MPa√m the R doesn't present any significate effect.

The results of the fatigue crack propagation in the stable regime were modeled by Paris law equation. Table 3 summarizes the values of the coefficients and intervals of validity of Paris' law and the correlation coefficients for all test conditions.

In order to analyze the transient effects after overloads they were carried out variable amplitude loading with R = 0.04 in which periodic overload blocks of 300 cycles were applied with intervals of N_{int} of 7,500 and 15,000 cycles as shown in Fig 3. The results obtained were compared with the reference constant amplitude loading tests. Figs 10 a) to 10 d) show the collected results from the tests performed in specimens with 8 mm thick. The typical transient behavior after overloads is not detected in all blocks because of the reduced transient zone and the crack measuring method. The analysis of the figure shows that for MP specimens the fatigue crack growth rate reduction reaches the maximum value for N_{int} = 7,500 cycles, while for the SP specimens the crack growth rate continues to decrease, although slightly, when N_{int} increases from 7,500 to 15,000 cycles.

For a better understanding of the fatigue mechanisms processes, the fractured surfaces of the samples were observed in a Philips XL30 scanning electron microscope. Fig. 11 shows two exemplary photos with different magnification of the crack propagated region

in Paris' law regime, representative of various observations done during the study. Both images from Fig. 11 show that propagation occurs mainly by striation.

4. Conclusions

The present work studied the effects of the shot peening and the stress ratio on the fatigue crack propagation of the 7475 aluminum alloy with a T7351 heat treatment, using two specimens' thickness: 4 and 8 mm. The analysis of the results drawn the follow conclusions:

- As a result of its small influence depth, the beneficial effect of shot peening on *da/dN-ΔK* curves is negligible, particularly for R = 0.4. However, this effect seems to increase near the threshold condition;

- For both mechanical polished and shot-peened samples, the specimens' thickness has only marginal influence on the stable crack propagation regime;

- A significant effect of the mean stress was observed, particularly in near- threshold region;

- Periodic overload blocks promotes a reduction of the fatigue crack growth rate. For MP specimens the reduction reaches the maximum value for the interval between blocks of 7,500 cycles, while for the SP specimens the crack growth rate continues to decrease, for intervals of 15,000 cycles.

Acknowledgements

This research is sponsored by FEDER funds through the program COMPETE – Programa Operacional Factores de Competitividade – and by national funds through FCT – Fundação para a Ciência e a Tecnologia –, under the project PEst-C/EME/UI0285/2013. The authors would like to acknowledge also OGMA-Indústria Aeronáutica de Portugal, Alverca, Portugal, and also Dra Ana Guimarães and Eng. João Miranda for the collaboration in the shot-peening processing.

References

[1] Fathallah R, Laamouri A, Sidhom H, Braham C.; High cycle fatigue behavior prediction of shot-peened parts. Int J Fatigue 2004; 26:1053–67.

[2] K. Miková, S. Bagherifard, O. Bokůvka, M. Guagliano, L. Trško, Fatigue behavior of X70 microalloyed steel after severe shot peening, Int. J. Fatigue. 55 (2013) 33-42.

[3] Bagherifard S., Guagliano M., Fatigue behavior of a low alloy steel with nanostructured surface obtained by severe shot peening, Eng. Fract. Mech. 81 (2012) 56-68.

[4] Zhang P., Lindemann J., Leyens L., Shot peening on the high-strength magnesium alloy AZ80 - effect of peening media. J. Mater. Process. Technol. 210 (2010) 445-450.

[5] Petit J, Mendez J. Some aspects of the influence of microstructure on fatigue resistance. Fatigue 96: Proceedings of the Sixth International Fatigue Congress, Vol. I. Lutjering G, Nowack H. (eds). Oxford: Pergamon 1996; p. 15-26.

[6] Bergner F., Zouhar G. A new approach to the correlation between the coefficient and the exponent in the power law equation of fatigue crack growth. Int J Fatigue 2000; 22: 229-239.

[7] Bergner F., Zouhar G., Tempus G.; The material-dependent variability of fatigue crack growth rates of aluminium alloys in the Paris regime. Int J Fatigue 2001; 23: 383-394.

[8] Sunder R., Dash P.K.; Measurement of fatigue crack closure through electron microscopy. Int J Fatigue 1982;4 (2):97–105.

[9] Zhou J.Z., Huang S., Sheng J., Lu J.Z., Wang C.D., Chen K.M., et al.; Effect of repeated impacts on mechanical properties and fatigue fracture morphologies of 6061-T6 aluminium subject to laser peening. Mater Sci Eng A 2012; 539:360–8.

[10] Pant B.K., Pavan A.H.V., Prakash R.V., Kamaraj M., Effect of laser peening and shot peening on fatigue striations during FCGR study of Ti6Al4V, International Journal of Fatigue 93 (2016) 38–50

[11] Vecchio R.S., Hertzberg R.W., Jaccard R.; On the overload induced fatigue crack propagation behavior in aluminium and steel alloys. Fatigue Engng Mater Struct 1984;7 (3):181–94.

[12] Ward-Close C.M., Blom A.F., Richie R.O.; Mechanisms associated with transient fatigue crack growth under variable amplitude loading: an experimental and numerical study. Engng Fract Mech 1989;32 (4):613–38.

[13] Krumar R., Garg S.B.L.; Effect of yield strength and single overload cycles on effective stress intensity range ratio in 6061-T6 Alalloy. Engng Fract Mech 1989;34 (2):403–12.

[14] Ling M.R., Schijve J.; The effect of intermediate heat treatments on overload induced retardations during fatigue crack growth in an Al-alloy. Fatigue Fract Engng Mater Struct 1992;15 (5):421–30.

[15] Damri D., Knott J.F.; Fracture modes encountered following the application of a major tensile overload cycle. Int J Fatigue 1993;15 (1):53–60.

[16] Shuter D.M., Geary W.; Some aspects of fatigue crack growth retardation behaviour following tensile overloads in a structural steel. Fatigue Fract Engng Mater Struct 1996;19 (2/3):185–99.

[17] Robin C., Louah M., Pluvinage G.; Influence of the overload on the fatigue crack growth in steels. Fatigue Fract Engng Mater Struct 1983;6 (1):1–13.

[18] Shercliff H.R., Fleck N.A.; Effect of specimen geometry on fatigue crack growth in plane strain—II. Overload response. Fatigue Fract Engng Mater Struct 1990;13 (3):297–310.

[19] Shin C.S., Hsu S,H.; On the mechanisms and behaviour of overload retardation in AISI 304 stainless steel. Int J Fatigue 1993;15 (3):181–92.

[20] Dexter R.J.; Hudak S.J., Davidson D.L.; Modelling and measurement of crack closure and crack growth following overloads and underloads. Engng Fracture Mech 1989;33(6):855–70.

[21] Tsukuda H., Ogiyama H., Shiraishi T.; Transient fatigue crack growth behaviour following single overloads at high stress ratios. Fatigue Fract Engng Mater Struct 1996;19(7):879–91.

[22] Borrego L.P., Ferreira J.M., Pinho da Cruz J.M., Costa J.M.; Evaluation of overload effects on fatigue crack growth and closure. Engineering Fracture Mechanics 70 (2003) 1379–1397.

[23] Donald K., Paris P.C.; An evaluation of DKeff estimation procedures on 6061-T6 and 2024-T3 aluminium alloys. Int J Fatigue 1999;21 (Supplement):S47–57.

[24] Paris P.C., Tada H., Donald J.K.; Service load fatigue damage—a historical perspective. Int J Fatigue 1999;21(Supplement):S35–46.

[25] Borrego L.P., Ferreira J.M., Costa J.M.; Fatigue crack growth and crack closure in an AlMgSi alloy. Fatigue Fract Engng Mater Struct 2001;24 (4):255–65.

[26] The American Standard SAE J443; Procedures for using standard shot peening test strip, 1968.

[27] The American Standard; Aerospace Materials Division, SAE, Shot Peening, 2009SAE AMS 2430.

[28] American Society for Testing and Materials. Standard test method for microhardness of materials. Annual Book of ASTM Standards 2000: Volume 03.01, ASTM E 647.

[29] DIN EN ISO 4288: Geometrical Product Specifications (GPS); Surface texture: Profile method; Rules and procedures for the assessment of surface texture; (1996).

[30] Standard Test Method for Vickers Indentation Hardness of Advanced Ceramics, ASTM C1327 (2015).

[31] Borrego L.P., Costa J.D.M., Silva S. and Ferreira J.M.; Microstructure dependent fatigue crack growth in aged hardened aluminium alloys, Int. Journ. Fatigue, Vol.26, pp. 1321 – 1331, 2004.

[32] He B.Y., Soady K.A., Mellor B.G., Gary Harrison, P.A.S. Reed, Fatigue crack growth behaviour in the LCF regime in a shot peened steam turbine blade material, Int. Journ. Fatigue, Vol.82, pp. 280–291. 2016.

Table 1 - Chemical composition of the 7475-T7351 aluminum alloy [% Weight].

Si	Fe	Cu	Mn	Mg	Cr	Zn	Ti	Others	Al
0.1	0.12	1.2-1.9	0.06	1.9-2.6	0.18-0.25	5.2-6.2	0.06	0.15	Remaining

Table 2 - Surface roughness parameters.

Specimen	**Parameter**	**Mean Value ± Standard Deviation** (μm)
MP	Ra	1,22±0,02
	Rq	1,50±0,02
	Rz	7,74±0,13
SP	Ra	3,70±0,17
	Rq	4,60±0,21
	Rz	23,50±2,00

Table 3 - Paris law parameters, *C* and *m* determined from *da/dN* versus *ΔK* curves [mm/cycle; MPa $m^{1/2}$].

B [mm]	Specimen	R	C	m	Validity [MPa $m^{1/2}$]	Correlation factor
4	MP	0.05	$1.41x10^{-8}$	3.94	7-13	0.995
4	MP	0.4	2.42×10^{-6}	2.04	12-24	0.996
4	SP	0.05	2.95×10^{-7}	2.94	8-14	0.970
4	SP	0.4	2.70×10^{-7}	3.05	5-10	0.982
8	MP	0.05	2.72×10^{-8}	3.89	7-12	0.996
8	MP	0.4	1.96×10^{-6}	2.16	13-22	0.998
8	SP	0.05	2.53×10^{-7}	2.97	9-16	0.991
8	SP	0.4	2.63×10^{-7}	3.25	5-17	0.973

Peer-reviewed version available at Appl. Sci. 2018, 8, 375; doi:10.3390/app8030375

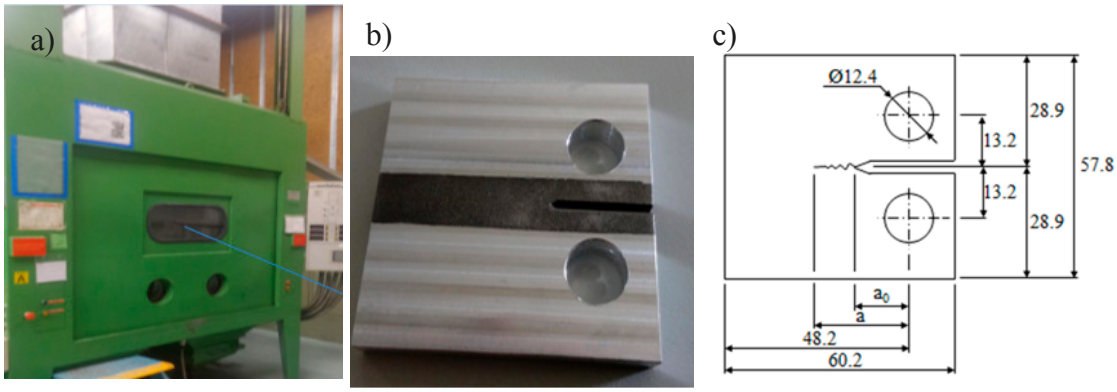

Figure 1 - a) Shot peening machine; b) shot peened specimen; c) dimensions of CT specimens.

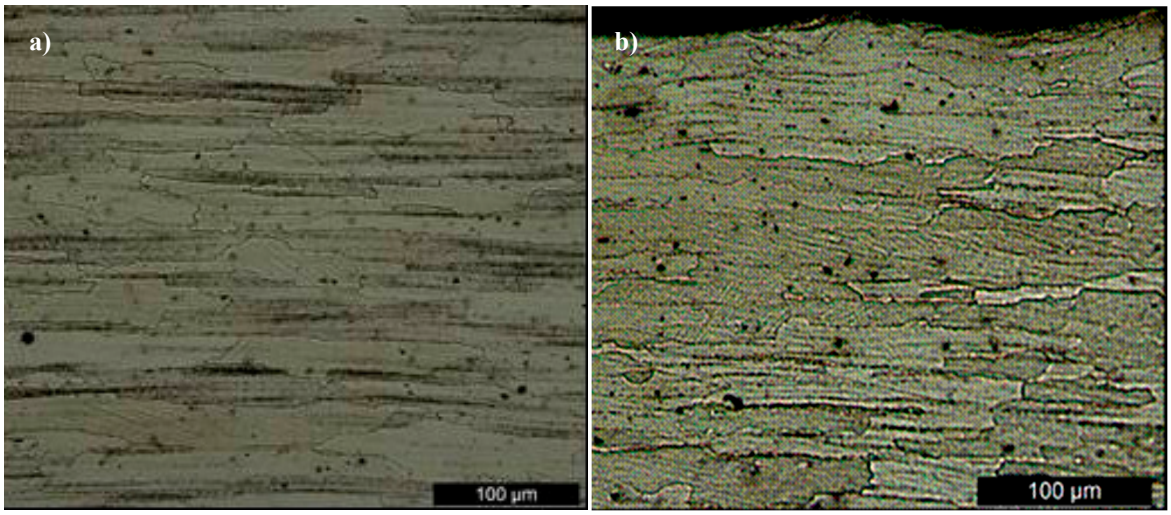

Figure 2 - Microstructure: a) base material; b) SP sample.

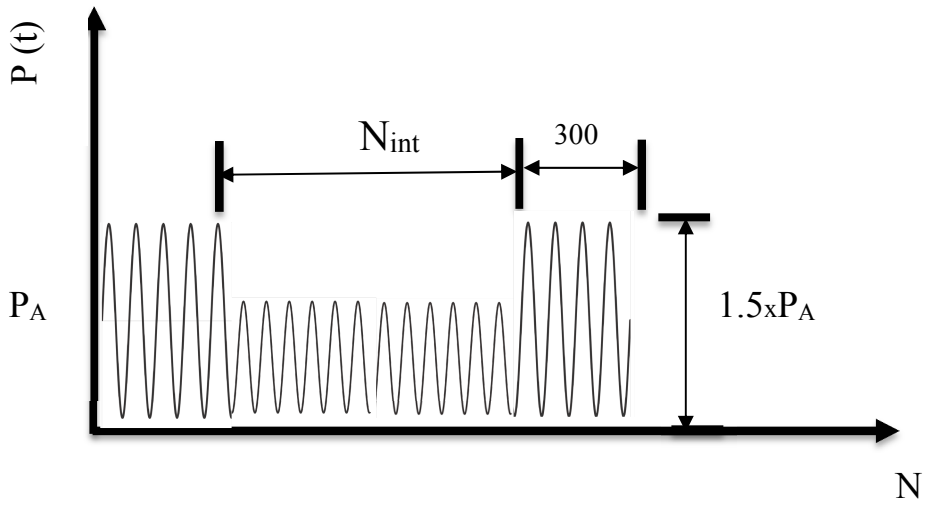

Figure 3 - Scheme of variable amplitude loadings with periodic overloading blocks.

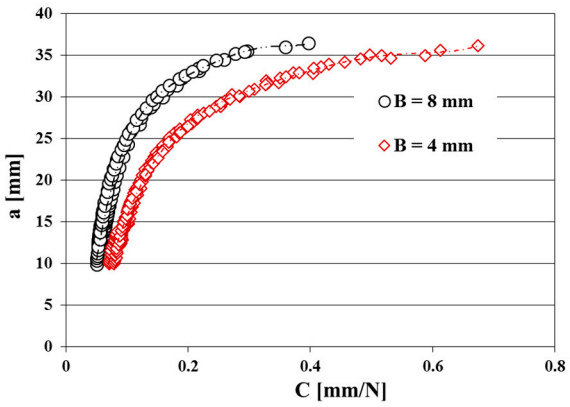

Figure 4 - Calibration curves based on the compliance, *C*, for both specimens with 4 and 8 mm thick.

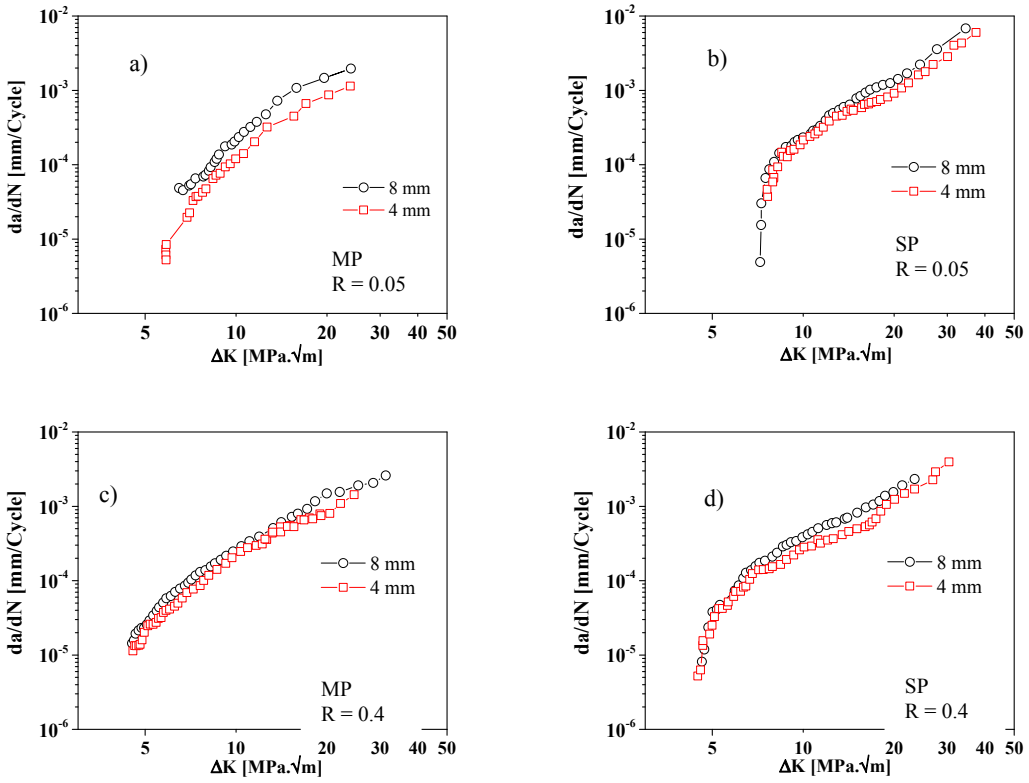

Figure 5 - Influence of the thickness on the *da/dN*-Δ*K* curves: a) MP, R = 0.05; b) SP, R = 0.05; c) MP, R = 0.4; d) SP, R = 0.4.

Preprints (www.preprints.org) | NOT PEER-REVIEWED | Posted: 24 January 2018 doi:10.20944/preprints201801.0219.v1

Peer-reviewed version available at Appl. Sci. 2018, 8, 375; doi:10.3390/app8030375

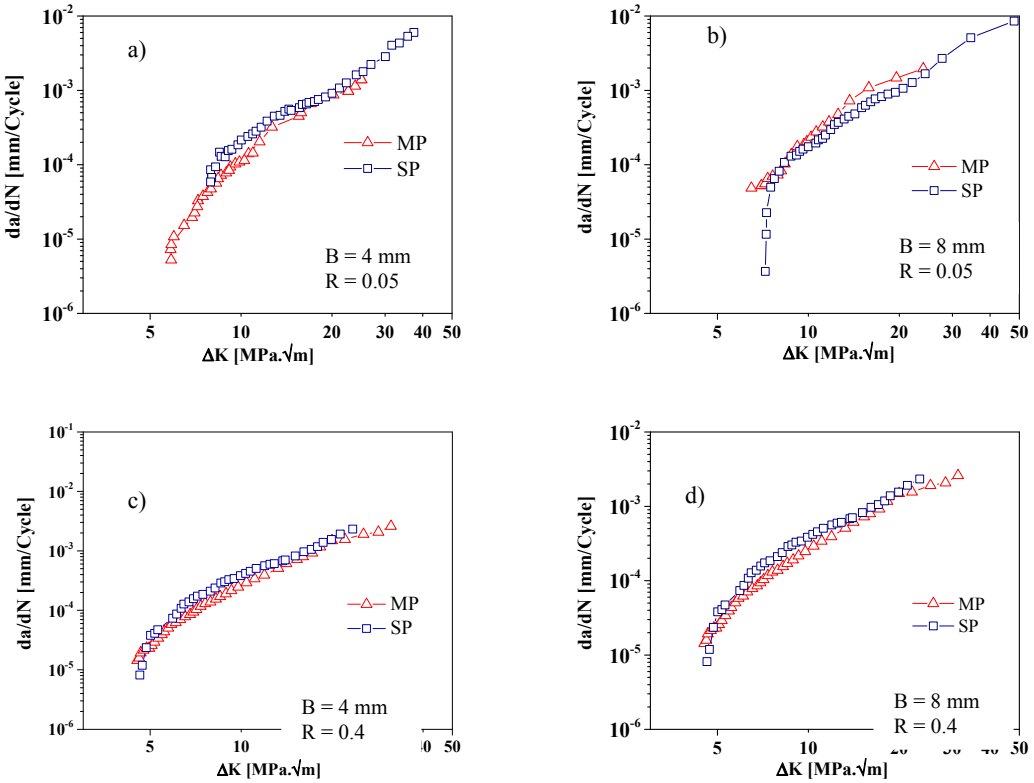

Figure 6 - Influence of the shot peening on the *da/dN*-Δ*K* curves a) B = 4 mm, R = 0.05; b) B = 8mm, R = 0.05; c) B = 4 mm, R=0.4; d), B = 8mm, R = 0.4.

Preprints (www.preprints.org) | NOT PEER-REVIEWED | Posted: 24 January 2018 doi:10.20944/preprints201801.0219.v1

Peer-reviewed version available at Appl. Sci. 2018, 8, 375; doi:10.3390/app8030375

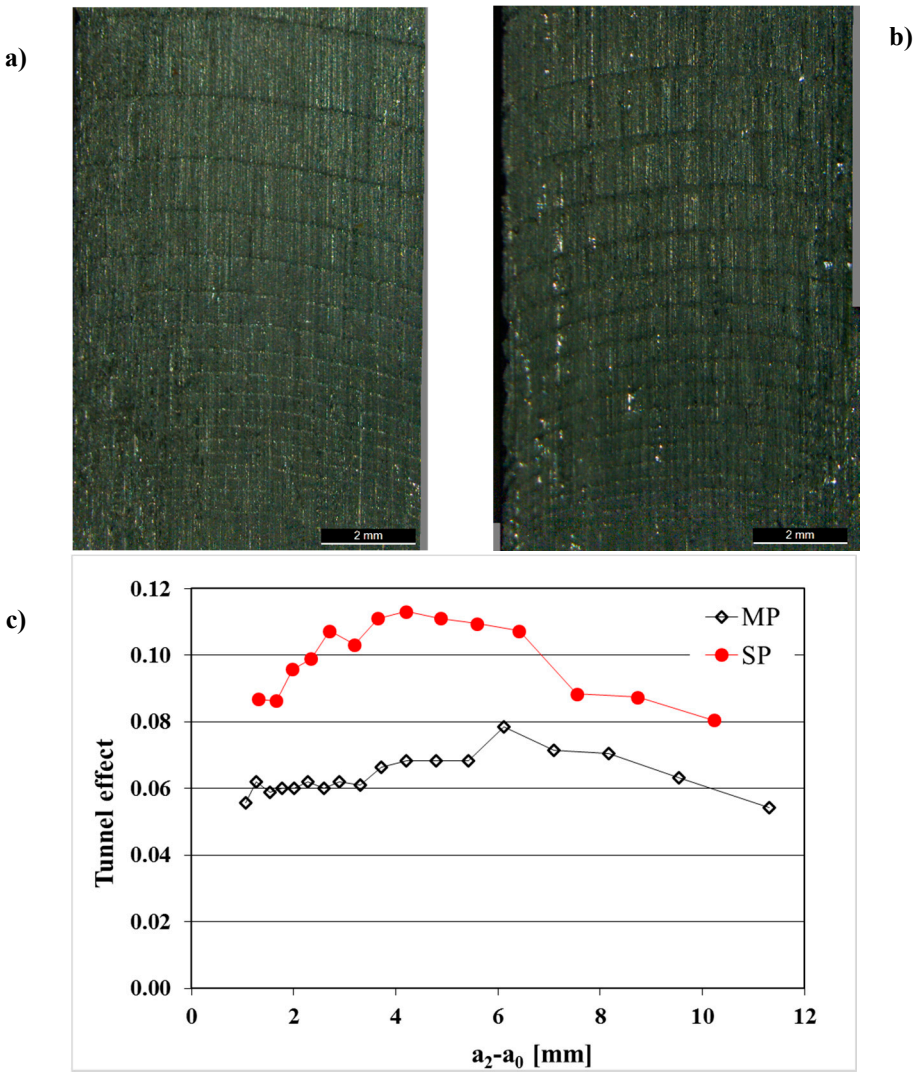

Figure 7 - Marks of the crack path and tunnel effect: a) MP specimens, b) SP specimens, Tunnel effect parameter.

Preprints (www.preprints.org) | NOT PEER-REVIEWED | Posted: 24 January 2018 doi:10.20944/preprints201801.0219.v1

Peer-reviewed version available at Appl. Sci. 2018, 8, 375; doi:10.3390/app8030375

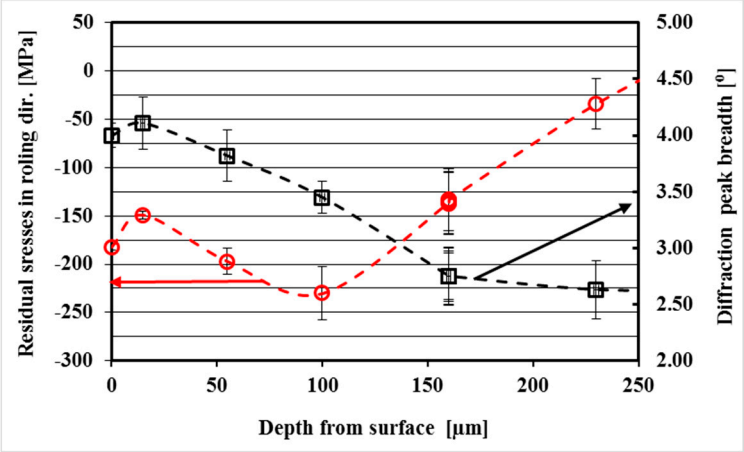

Figure 8 – Residual stresses profile and X-ray diffraction peak breadth against the depth from surface for SP specimens.

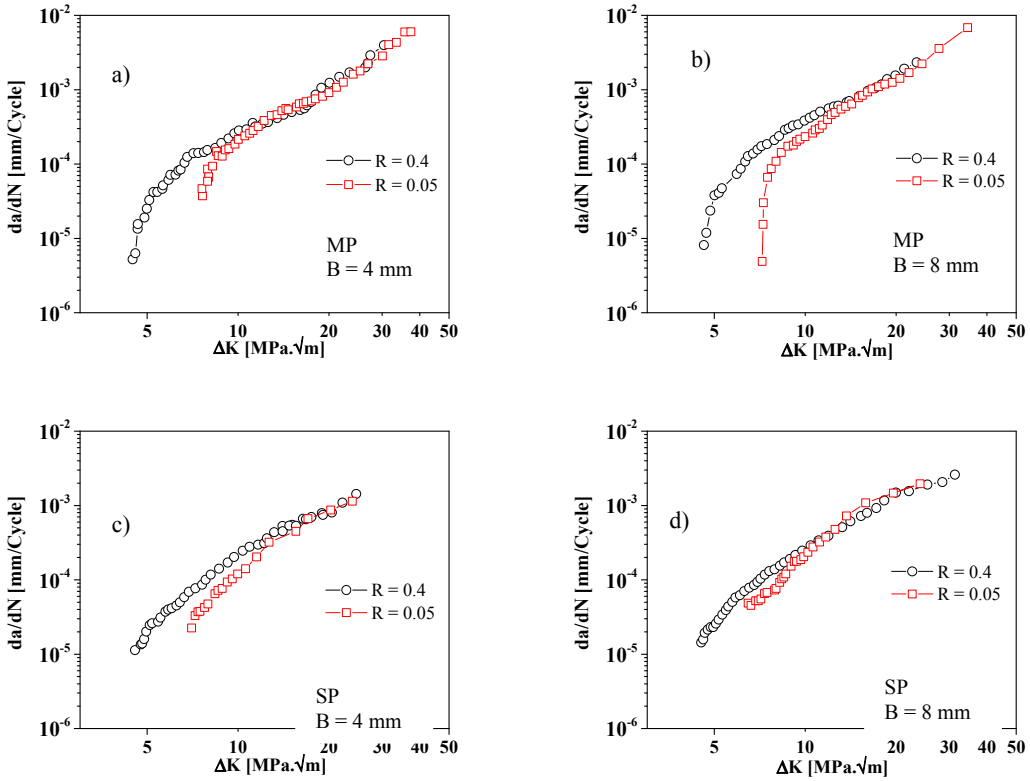

Figure 9 - Influence of *R* on the *da/dN*-Δ*K* curves: a) *B* = 4 mm, *MP*; b) *B* = 8 mm, *MP*; c) *B* = 4 mm, *SP*; d), *B* = 8 mm, *SP*.

Preprints (www.preprints.org) | NOT PEER-REVIEWED | Posted: 24 January 2018 doi:10.20944/preprints201801.0219.v1

Peer-reviewed version available at Appl. Sci. 2018, 8, 375; doi:10.3390/app8030375

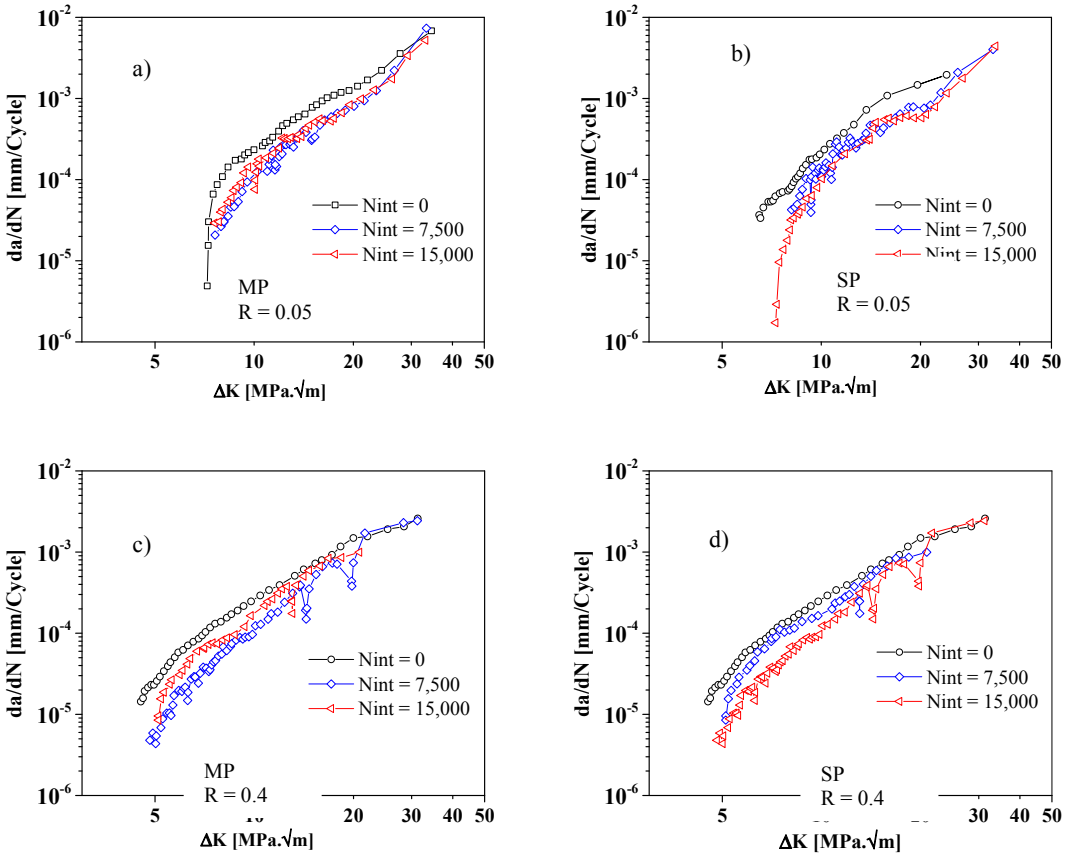

Figure 10 - Influence of block overload on the *da/dN*-Δ*K* curves for 8 mm thick specimens: a) R = 0.05, SP; b) R = 0.05, MP; c) R = 0.4, SP; d) R = 0.4, MP.

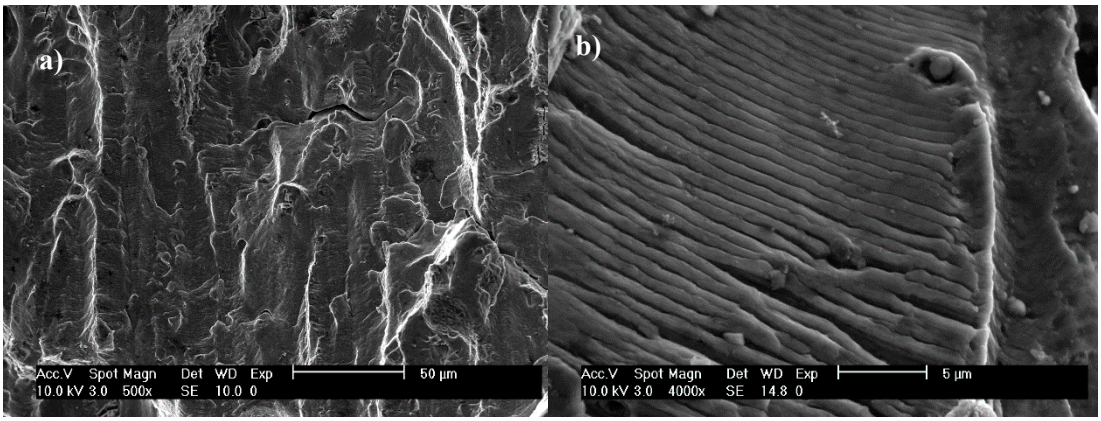

Figure 11 - Exemplary fracture surface morphology from SEM observations.